KYBERNETIKA — VOLUME *49* (2013), NUMBER 2, PAGES 301–318

SEGMENTATION OF MRI DATA BY MEANS OF NONLINEAR DIFFUSION

Radomír Chabiniok, Radek Máca, Michal Beneš and Jaroslav Tintěra

The article focuses on the application of the segmentation algorithm based on the numerical solution of the Allen-Cahn non-linear diffusion partial differential equation. This equation is related to the motion of curves by mean curvature. It exhibits several suitable mathematical properties including stable solution profile. This allows the user to follow accurately the position of the segmentation curve by bringing it quickly to the vicinity of the segmented object and by approaching the details of the segmentation curve. The purpose of the article is to indicate how the algorithm parameters are set up and to show how the algorithm behaves when applied to the particular class of medical data. In detail we describe the algorithm parameters influencing the segmentation procedure. The left ventricle volume estimated by the segmentation of scanned slices is evaluated through the cardiac cycle. Consequently, the ejection fraction is evaluated. The described approach allows the user to process cardiac cine MR images in an automated way and represents, therefore, an alternative to other commonly used methods. Based on the physical and mathematical background, the presented algorithm exhibits the stable behavior in the segmentation of MRI test data, it is computationally efficient and allows the user to perform various implementation improvements.

Keywords: degenerate diffusion, Allen–Cahn equation, image segmentation, magnetic resonance imaging

Classification: 80A22, 82C26, 35A40, 68U10

1. INTRODUCTION

The methods of image analysis have an increasing importance in the processing of the MRI data related to the segmentation of various parts of human body, e. g. the myocardium or the brain. Generally, the segmentation is performed using various techniques as described in [6]. A longterm research activity was devoted to the variational formulation [18, 20], statistical analysis [11, 23], combinatorics [7], curve motion [14, 17] or nonparametric clustering [9]. The approach described in the presented article belongs to the class of diffusion-based segmentation methods (see [10, 16, 17]).

Currently, magnetic resonance imaging (MRI) devices provide rather large data sets. Therefore, their efficient processing requires automated procedures. The examination of heart function by means of the cine MRI gained its importance due to the accuracy of provided information. It is represented by several hundreds of 2D MR images covering the left ventricle (LV) volume throughout the cardiac cycle interval with the time

resolution achieving 20–40 ms.

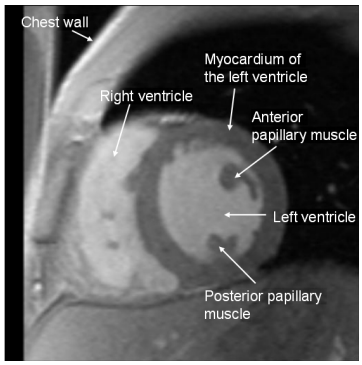

(a) Time frame 01 (heart contraction).

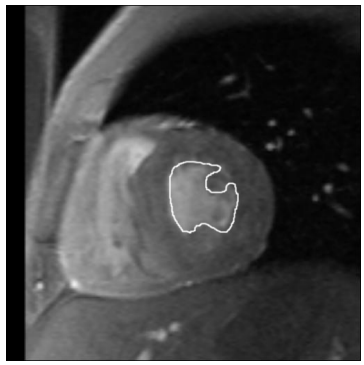

(b) Time frame 09 (end-systole). Inner contour of the ventricle volume (papillary muscles are excluded).

Fig. 1. Example of cardiac MR images – cine series of the heart in short axis view.

In Figure 1, the example of cardiac cine MRI in the short axis projection is presented. The slice corresponds to the mid-cavity part of LV, with the time frame 01 acquired in the end-diastole (maximum ventricle volume) and the time frame 09 in the end-systole (minimum ventricle volume). The total number of images from a single examination exceeds 100. The segmentation is usually required for all images. For details of the cardiac MRI, see e. g. [5].

The segmentations of the LV volume and of the LV wall are considered the important part of the cine MRI processing. They allow the user to estimate several hemodynamic parameters, as for instance the LV ejection fraction, the stroke volume or the kinetic parameters of the wall thickening.

The article has the following contents. The segmentation method is described. It is based on the edge detection by means of nonlinear diffusion. The segmentation algorithm operates on a certain range of parameters described in the text. Their choice is given partially by the physical context of the algorithm, and partially by the experience with applications. The sample results of the cine MRI data processing are presented and discussed.

2. NONLINEAR DIFFUSION AND THE ALLEN–CAHN EQUATION

The presented segmentation algorithm is based on the iterative segmentation approximation of the area of interest by means of a numerically solved nonlinear transient diffusion equation of the Allen–Cahn type (see [1]). The iteration from the initial guess to the final approximation of the object contour is controlled by the intensity of the processed image and by its spatial gradient.

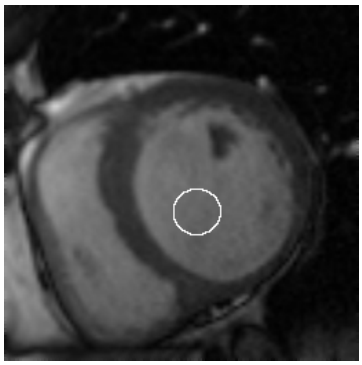

(a) Initial position of the segmentation curve.

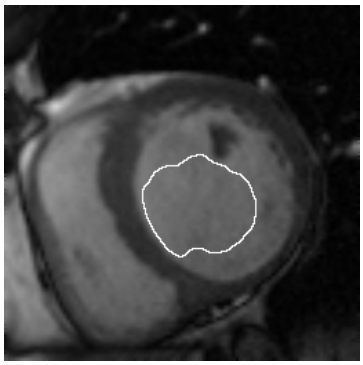

(b) Position of the segmentation curve for $t = 0.0015$.

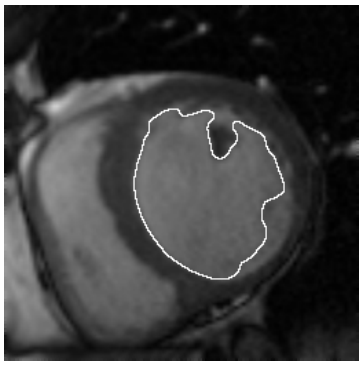

(c) Position of the segmentation curve for $t = 0.0061$.

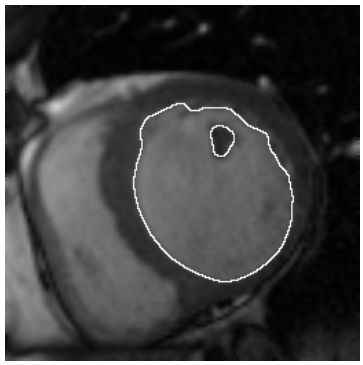

(d) Position of the segmentation curve for $t = 0.0148$.

Fig. 2. Evolution of the segmentation curve for a given slice and time frame of Subject 1.

The mentioned diffusion process is derived by the phase-field approach to the mean curvature flow (see e. g. [3]). The main principles of this method can be summarized as follows. We denote the segmentation function by $p(t, x)$. The function $p(t, x)$ evolves according to the following initial-boundary-value problem for the modified Allen–Cahn equation (see [1]):

$$\begin{aligned} \xi \frac{\partial p}{\partial t} &= \xi \nabla \cdot \left(g\left(|\nabla P_0|\right) \nabla p \right) + g\left(|\nabla P_0|\right) \left(\frac{1}{\xi} f_0(p) + \xi F |\nabla p| \right) \text{ in } (0,T) \times \Omega, \quad (1) \\ p\,|_{\partial\Omega} &= 0 \quad \text{ on } (0,T) \times \partial\Omega, \\ p|_{t=0} &= p_{ini} \text{ in } \overline{\Omega}, \end{aligned}$$

where $\Omega = (0, L_1) \times (0, L_2) \subset \mathbb{R}^2$, $L_1 > 0$, $L_2 > 0$ stands for a rectangular area representing the processed image, the spatial variable $x = [x_1, x_2] \in \bar{\Omega}$, $t \in \langle 0, T \rangle$ is a

variable parameterizing the conversion of the initial guess p_{ini} of the segmented area into its final shape represented by the solution of (1) evaluated at $t = T$. Due to the physical context of (1), we speak of t as of the time variable. Other quantities are explained below.

The function $p(t, x)$ – the solution of (1) – has its values in $\langle 0, 1\rangle$ which is guaranteed by the particular form of the polynomial function f_0 having the values of 0 and 1 as roots. More details can be found e. g. in [3]. The segmentation curve at time t is given by the level set

$$\Gamma(t) = \left\{ x \in \Omega : p(t, x) = \frac{1}{2} \right\}.$$

The thickness of the transition layer between the values of $p = 0$ and $p = 1$ is given by the small parameter $0 < \xi \ll 1$. The profile of p across $\Gamma(t)$ remains stable for all t. When $\xi \to 0_+$, the segmentation curve $\Gamma(t)$ evolves according to the mean-curvature evolution law.

This fact is given by the relationship described briefly here, in [2] and in references therein more in detail. The mean-curvature flow is governed by the motion law for the curve Γ in direction of its normal vector

$$v_\Gamma = -\kappa_\Gamma + F, \tag{2}$$

where v_Γ stands for the normal velocity of Γ, κ_Γ is the curvature of Γ, and F has the meaning of the external force influencing the motion. The motion law (2) clarifies the function of the segmentation algorithm considered here.

Using the matched asymptotic expansions, the relationship between (1) and (2) is recovered for $\xi \to 0$ when the level set $\Gamma(t)$ moves according to (2). The asymptotical behaviour is schematically expressed as follows:

$$\begin{array}{ccccccc} \underbrace{\xi \dfrac{\partial p}{\partial t}} & = & \underbrace{\xi \Delta p + \dfrac{1}{\xi} f_0(p)} & + & \underbrace{\xi F |\nabla p|} \\ \downarrow & & \downarrow & & \downarrow \\ v_\Gamma & = & -\kappa_\Gamma & + & F \end{array}$$

and is analyzed e. g. in [2] and in references therein.

The initial guess of the segmented area $p(0, x) = p_{ini}(x)$ can be given by the characteristic function of the initial segmented area. In the given context, an automated choice of p_{ini} becomes convenient, as discussed in Section 4.2.

The intensity of the MR signal in the segmented image controls the algorithm by means of the function $P_0(x)$. This function is the convolution of the piecewise constant signal intensity of the MR image with the Gaussian smoothing kernel with a suitable variance corresponding to the neighborhood width of several pixels. Resulting values are in the interval of $\langle 0, 255\rangle$. Other terms in Equation (1) are described in the following manner:

- $g : \mathbb{R}_0^+ \to \mathbb{R}^+$ is the Perona–Malik function (see [3] and references therein), with the property $g(s) \to 0$ as $s \to +\infty$. Our choice is $g(s) = \frac{1}{1+\lambda s^2}$ with the parameter $\lambda > 0$.

- F originally meant an external force that quickly brought the segmentation curve to the vicinity of the segmented object. The sign of F causes either the expansion of the segmented area (for $F > 0$) or the shrinkage (for $F < 0$). The improved choice of F is described in Section 4.2

- $f_0(p) = p(1-p)(p-\frac{1}{2})$ is the polynomial given by the phase-field theory (see [1,2]).

The segmentation function $p(t, x)$ is evolved by the diffusion process described by Equation (1). As a consequence, the segmentation curve $\Gamma(t)$ approaches the edges of the objects of interest (see Figure 2). The segmentation process terminates for a suitable value $t = T$ when no substantial change in p is observed. Details are described in the following sections. Problem (1) is well posed. In [3], in agreement with [2], it is shown that it possesses the unique weak solution with corresponding regularity.

The mathematical context of the problem given by Equation (1) implies that motion of the segmentation curve is smooth and stable, as given by the results of [2, 3] and of references therein. Additionally, the above described approach is related to the level set methods since the curve Γ for $\xi \to 0_+$ evolves by the same law as the level sets of the solution of the level set equation, as discussed in [2,19]. In this sense, problem (1) is the alternative to the level set equation for the segmentation function studied e. g. in [15]. In Section 5, the level set equation is used as one of comparison tools for the presented algorithm.

3. SEGMENTATION ALGORITHM

The segmentation algorithm is based on the numerical solution of problem (1) by means of the finite-difference method. Problem (1) is approximated on a rectangular uniform spatial grid and with a constant time step. The processed image data is bilinearly interpolated in order to obtain corresponding data on an arbitrary numerical grid.

Denoting τ the segmentation time step, h_1, h_2 the mesh sizes with the corresponding numbers of nodes N_1, N_2 in directions x_1, x_2, and $p^k_{i,j}$ values of function p at $x = [ih_1, jh_2]$, $t = k\tau$, the semi-implicit finite-difference scheme for problem (1) has the following form

$$\xi \mathbf{A}\mathbf{p} - \frac{\tau}{\xi}\mathbf{f}(\mathbf{p}) = \xi \mathbf{F}, \tag{3}$$

where

$$\begin{aligned}
\mathbf{p} &= p^k_{i,j}, \\
\mathbf{A}\mathbf{p} &= p^k_{i,j} - \frac{\tau}{h_1^2}\left(g_{i+1,j}\left(p^k_{i+1,j} - p^k_{i,j}\right) - g_{i,j}\left(p^k_{i,j} - p^k_{i-1,j}\right)\right) \\
&\quad - \frac{\tau}{h_2^2}\left(g_{i,j+1}\left(p^k_{i,j+1} - p^k_{i,j}\right) - g_{i,j}\left(p^k_{i,j} - p^k_{i,j-1}\right)\right), \\
\mathbf{f}(\mathbf{p}) &= g_{i,j} f_0\left(p^k_{i,j}\right), \\
\mathbf{F} &= p^{k-1}_{i,j} + \tau g_{i,j} F_{i,j}\Big(\Big(\frac{1}{h_1}(p^{k-1}_{i,j} - p^{k-1}_{i-1,j})\Big)^2 + \Big(\frac{1}{h_2}(p^{k-1}_{i,j} - p^{k-1}_{i,j-1}))^2\Big)^{\frac{1}{2}},
\end{aligned}$$

for $i = 1 \ldots N_1 - 1$, $j = 1 \ldots N_2 - 1$.

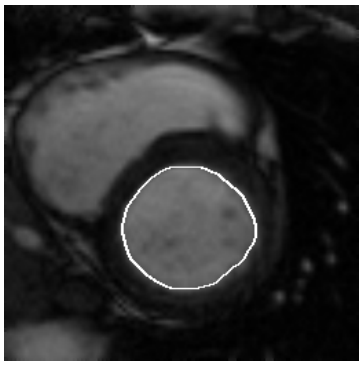

(a) Slice 04, time frame 03.

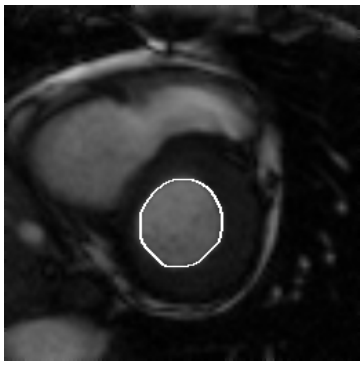

(b) Slice 04, time frame 09 (end-systole).

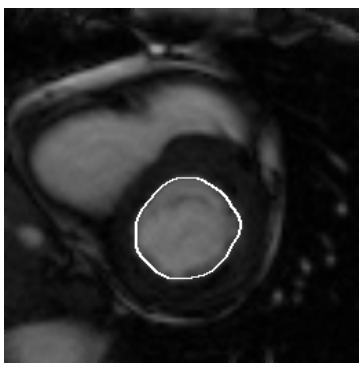

(c) Slice 04, time frame 11.

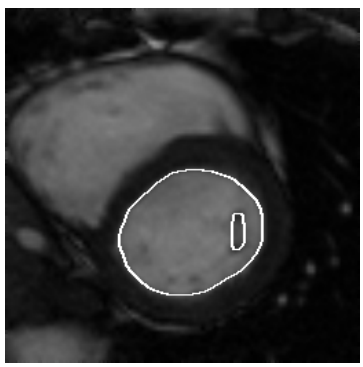

(d) Slice 04, time frame 22 (end-diastole).

Fig. 3. Segmentation of a given slice at selected time frame for Subject 3.

The details and properties of the numerical scheme are described in [3]. The system of nonlinear algebraic equations (3) is approximately solved with respect to $\mathbf{p}$ by means of the nonlinear Gauss–Seidel method described in [3]. The convergence issues are analyzed in [4].

The segmentation algorithm starts at the initial guess by setting $p^0_{i,j} = p_{ini}(ih_1, jh_2)$. The next iteration is obtained from (3) by setting $k = 1$. For each higher k, knowing the preceding iteration $p^{k-1}_{i,j}$, the following iteration is obtained from (3) again. This process terminates when $k\tau = T$.

4. MRI DATA SEGMENTATION PARAMETERS

In this section, we discuss the role of algorithm parameters and provide guidelines for their setting. The parameters can be divided into the following groups:

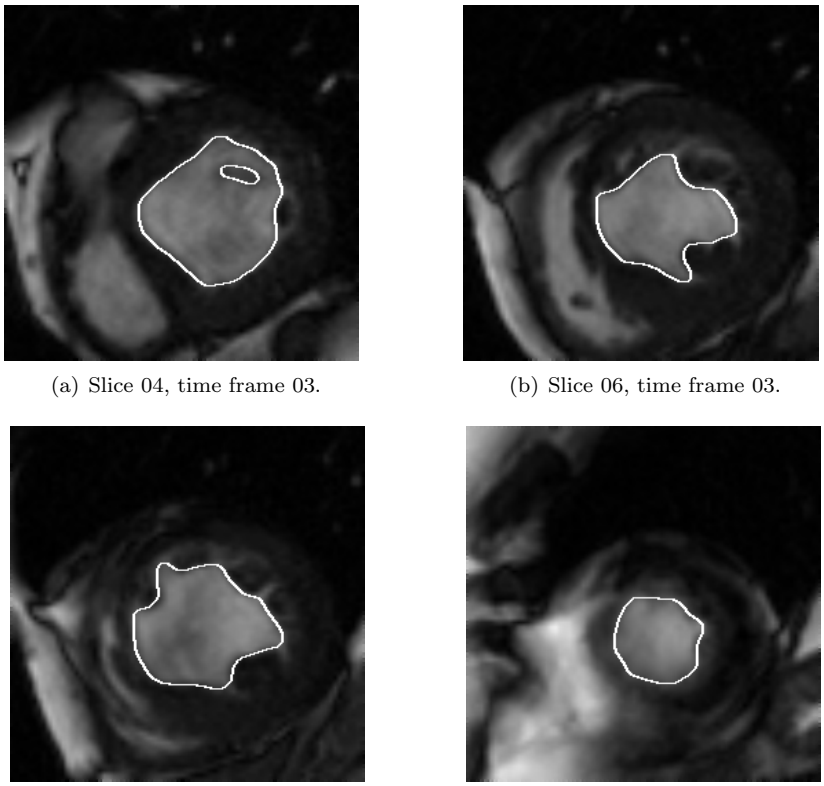

(a) Slice 04, time frame 03. (b) Slice 06, time frame 03.

(c) Slice 07, time frame 03. (d) Slice 10, time frame 03.

Fig. 4. Segmentation of a given frame at selected slices for Subject 5.

- physical parameters – the small diffusion parameter ξ, the domain size $L_{1,2}$, the force function F, the segmentation extent T (originally, the time extent) and the initial guess p_{ini};
- numerical parameters – the number of nodes $N_{1,2}$, the mesh size $h_{1,2}$, the number of segmentation iteration steps N_T, the segmentation (time) step τ;
- image parameters – the parameter in the Perona–Malik function λ, the mollified image data P_0.

The physical parameters are given by the original physical context regardless the segmentation task. Their values are given by the ranges used in various applications of the Allen–Cahn equation. This implies the choice of $L_{1,2}$ of the order of 1 (keeping the image aspect ratio), $\xi \approx 0.004$, which implies that the algorithm can recognize details of size $0.2\% - 1\%$ of the image size due to the role of this parameter in the solution of (1). By its sign the function F imposes the expansion or shrinkage of the initial curve. Due

to this role, it can be useful in bringing the segmentation curve close to the segmented object (see Section 4.2). The time extent T indicates when the segmentation terminates. For its choice, a criterion described in Section 4.3 is used. The initial condition p_{ini} is crucial for indicating the area which the segmented object belongs to. We, therefore, describe the details of the choice of F, T and p_{ini} below.

The numerical parameters are given by numerical scheme (3). The parameters $N_{1,2}$ are greater or equal to the image extent in pixels. Consequently, $h_{1,2} = L_{1,2}/N_{1,2}$. In the presented results, we set $h_{1,2} = 0.0039$, $N_{1,2} = 256$, $\xi = 0.004$. The parameter N_T is given by T , and $\tau = T/N_T$. In agreement with [3], the parameters satisfy the relations $h_{1,2} < \xi$ and $\tau < \text{const.}\,\xi^2$ required for proper function of numerical scheme (3).

The image parameters are given by the processing requirements. The mollified image is stored in P_0. The choice of the parameter λ is described below.

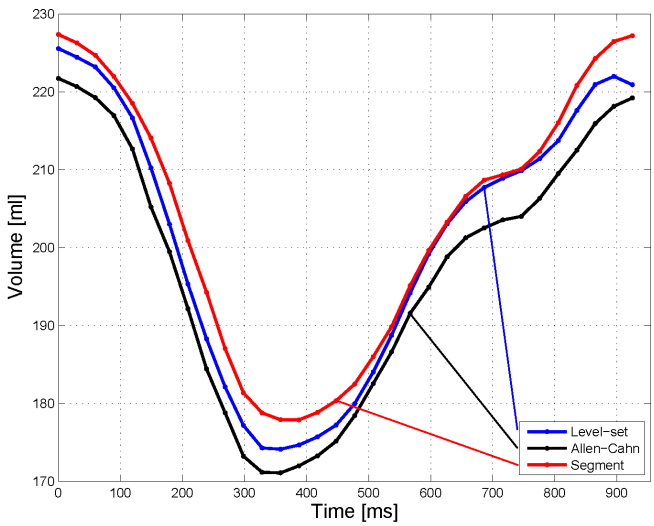

Fig. 5. Subject 1: Estimate of the LV volume during the heart cycle.

	EF	ESV	EDV
Allen–Cahn	22.83	171.08	221.70
Level-Set	22.80	174.12	225.54
Segment	21.75	177.89	227.34

Tab. 1. Subject 1: Comparison of the ejection fraction estimated by the described algorithm, the level set methods and the algorithm SEGMENT.

4.1. Perona–Malik function

The information carried by the processed image is incorporated into the algorithm by means of the Perona–Malik function g (originally described in [21]):

$$g(s) = \frac{1}{1 + \lambda s^2}, \text{ where } \lambda > 0. \tag{4}$$

The function g depends on the gradient magnitude of the image intensity ($|\nabla P_0|$). The large values of $|\nabla P_0|$ indicate possible edges in the image. In such regions the function g tends to 0. In the areas without edges, the intensity gradient is small and the function g is close to 1.

The algorithm sensitivity to detect edges depends on the value of λ. The smaller the parameter λ is, the higher the sensitivity is. This means that the low values of λ weaken the ability of the edge detection. However, the large values of λ can lead to the detection of spurious edges given by inhomogeneities of the signal due to the limited signal-to-noise ratio, blood flow artifacts, etc.

Equation (1) has the intrinsic smoothing property. The segmentation curve becomes smooth for any positive time. This is an important aspect for the practical application in segmentation. In real images, inhomogeneities can cause the partial absence of the edges (due to limited signal-to-noise ratio and time resolution). The missing edges can be approximated using the smoothing property of the algorithm. For this purpose, the parameter λ should not be very large. This choice is limited from below, as λ influences the edge detection.

Practical experience with various image data (see [3]) suggests using the values of λ between 1 and 30. In the presented results, we set $\lambda = 5$.

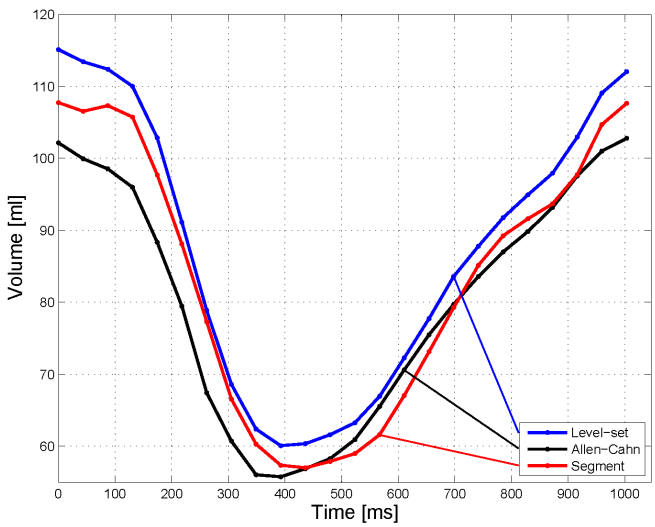

Fig. 6. Subject 2: Estimate of the LV volume during the heart cycle.

	EF	ESV	EDV
Allen–Cahn	45.74	55.76	102.76
Level-Set	47.81	60.08	115.11
Segment	47.09	57.00	107.73

Tab. 2. Subject 2: Comparison of the ejection fraction estimated by the described algorithm, the level set methods and the algorithm SEGMENT.

4.2. External force F and initial guess of segmented area

As mentioned in Section 2, the motion of segmentation curve $\Gamma(t)$ given by the evolution of the solution of (1) is related to evolution law (2).

In particular, negative v_Γ means the shrinkage and positive v_Γ means the expansion of the segmented area. Consequently, suitably chosen negative values of F can stimulate the shrinkage of the segmentation curve, suitably chosen positive values of F can stimulate the expansion of the segmentation curve towards the object of interest. However, this process is influenced by the curvature κ_Γ as well.

Therefore, the choice of F is connected to the choice of the initial guess p_{ini}. If the initial circular area covers the object of interest and F is negative, the segmentation curve quickly approaches the vicinity of the object of interest from outside. If the initial circular area is embedded into the object of interest and F is positive, greater than the curvature of the initial curve $\Gamma(0)$, the segmentation curve quickly approaches the vicinity of the object of interest from inside as in Figure 2.

In cardiac cine MR images, the segmentation results of neighboring slices in space and time can serve as the initial guess as well. Due to the misalignment of the slices acquired at different breath-holds, the initial guess p_{ini} is often partially in and partially out of the segmented object. If the initial guess covers a part of the ventricle volume and a part of the ventricle wall only, while keeping the external force F constant across the image, only some edges can be detected. These edges become a part either of the inner contour or of the outer contour of the myocardium. Other parts of edges can be missed, and therefore the ventricle can become uncompletely segmented. This difficulty can be solved by suggesting the dependence of F on the known features of the signal P_0.

In cardiac cine MR images the blood in the ventricles is lighter than the myocardium (the so-called 'light blood technique') and the surrounding lung tissue is the darkest part. Using a histogram analysis we can obtain rough thresholds for the signal intensities P_0 inside the cavity (a high intensity – threshold value I_{cavity}) and outside the heart (a low intensity - threshold value $I_{outside}$). Positive values of F for the positions inside the cavity (hence in the parts of the image with the intensity values above I_{cavity}) and negative values of F elsewhere would cause the segmentation – curve expanding if being inside the ventricle, or shrinking if being outside. Formally, we can prescribe the function F in the following manner:

$$F(x) = \begin{cases} 100 & \text{in } \{x \in \Omega; P_0(x) > I_{cavity}\} \\ -10 & \text{elsewhere.} \end{cases} \tag{5}$$

The function F defined according to (5) leads to the proper segmentation of the LV cavity. Such a formula is used in the presented results.

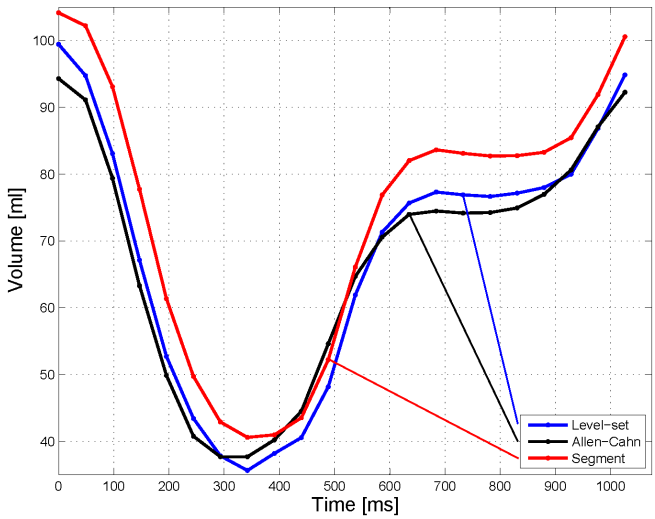

Fig. 7. Subject 3: Estimate of the LV volume during the heart cycle.

	EF	ESV	EDV
Allen–Cahn	60.05	37.67	94.28
Level-Set	64.16	35.63	99.42
Segment	61.03	40.58	104.13

Tab. 3. Subject 3: Comparison of the ejection fraction estimated by the described algorithm, the level set methods and the algorithm SEGMENT.

4.3. Stopping criterion

The above mentioned algorithm set-up makes the segmentation process dependent on the spatial gradient of the input image signal, and also on the magnitude of the input signal. There are various approaches to the choice of the value of t when the segmentation terminates. For example, a rule can be found in [3] and in references therein. It operates with a threshold for the change in p with respect to t.

In this article we suggest the following criterion. After each series of N iterations (N is for example 100) the segmented area is estimated (by counting the number of pixels in the area), and is compared with the estimated area before the N iterations. When the relative difference is less than a given threshold (such as 5%), the segmentation

is terminated. We also determine the maximum number of iterations, after which the segmentation terminates even if the 5% criterion is not satisfied.

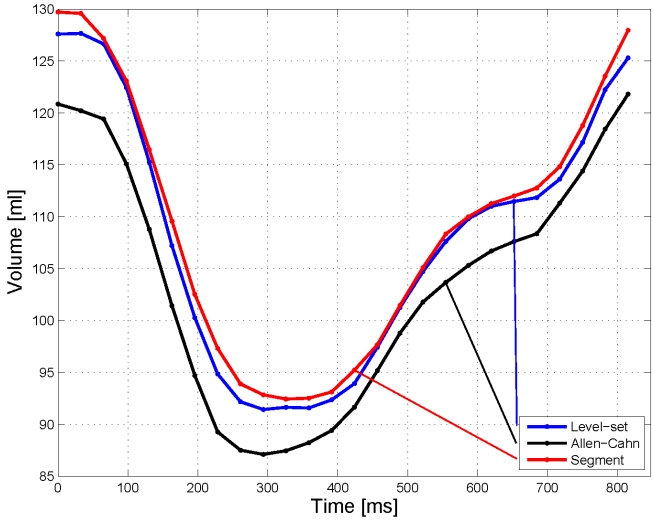

Fig. 8. Subject 4: Estimate of the LV volume during the heart cycle.

	EF	ESV	EDV
Allen–Cahn	28.48	87.11	121.80
Level-Set	28.38	91.43	127.66
Segment	28.74	92.43	129.71

Tab. 4. Subject 4: Comparison of the ejection fraction estimated by the described algorithm, the level set methods and the algorithm SEGMENT.

5. TEST DATA AND COMPARISON WITH OTHER METHODS

The MR data used for testing the algorithm were acquired by the 1.5T MR system (Siemens Avanto). The cardiac cine data were obtained in retrospective cardiac triggering in breath-hold periods using either balanced steady-state free precession acquisition sequence (bSSFP, trueFISP). Basic parameters of the bSSFP sequence were the following: flip angle = 70–80 °, TR $\sim$ 65 ms, turbo factor 24, TE $\sim$ 1.2 ms, echo spacing $\sim$ 2.7 ms, voxel size 2 x 1.6 x 8 mm, FOV 300 x 300 mm, bandwidth = 930 Hz/pixel, 20 – 40 frames per cardiac cycle.

The described algorithm has been compared to two other segmentation approaches - the level-set method described in [15] and the SEGMENT software available on [13].

The approach based on the level set formulation considers the motion of the segmentation curve $\Gamma(t)$ given by the level set of the field $u = u(t, x)$

$$\Gamma(t) = \{x \in \Omega \,|\, u(t, x) = 0\} \tag{6}$$

propagating in the normal direction according to (2). The function u then satisfies the equation

$$\frac{\partial u}{\partial t} = |\nabla u| \, \nabla \cdot \frac{\nabla u}{|\nabla u|} - |\nabla u| \, F \,. \tag{7}$$

In applications, the term $|\nabla u|$ is approximated as $\sqrt{\varepsilon^2 + |\nabla u|^2}$ with ε small (see e. g. [17]).

In the comparison, we use the modification of (7) proposed in [15]:

$$\begin{aligned} \frac{\partial u}{\partial t} &= g^0 |\nabla u|_\varepsilon \nabla \cdot \left(\frac{\nabla u}{|\nabla u|_\varepsilon} \right) + \mathcal{A} \nabla g^0 \cdot \nabla u - g^0 |\nabla u|_\varepsilon F, \\ u|_{t=0} &= d_{\Gamma_0}, \end{aligned} \tag{8}$$

where $g^0 = g\,(|\nabla P_0|)$, $\mathcal{A}$ is the balance parameter weighting the convection term in (8) and d_{Γ_0} is the signed distance function (see [15] and references therein) constructed for the initial curve $\Gamma(0)$.

The **SEGMENT** is a freely available software for cardiovascular image analysis. It can be used for the analysis of the MR data. The software provides the automated segmentation of the left ventricle as well as the manual and general object segmentation. The segmentation algorithm is based on the concept of deformable objects. The geometrical representation of an image object can be deformed under the internal deformation energy and the external potential energy field. The energy minimization is described by the Euler–Lagrange equations (see [12]). In our case, the SEGMENT algorithm was used to segment the LV cavity. Partially, manual corrections removed obvious mismatch with the LV boundary.

	EF	ESV	EDV
Allen–Cahn	25.22	61.13	81.75
Level-Set	24.66	62.68	83.19
Segment	24.46	62.10	82.21

Tab. 5. Subject 5: Comparison of the ejection fraction estimated by the described algorithm, the level set methods and the algorithm SEGMENT.

6. RESULTS OF VOLUME SEGMENTATION OF THE LV CAVITY

In this section, the cardiac MR data of 5 subjects provided by the Institute of Clinical and Experimental Medicine in Prague are examined. The data for the LV cavity volume segmentation consist of a series of 12 spatial slices and of 20–40 time frames per the

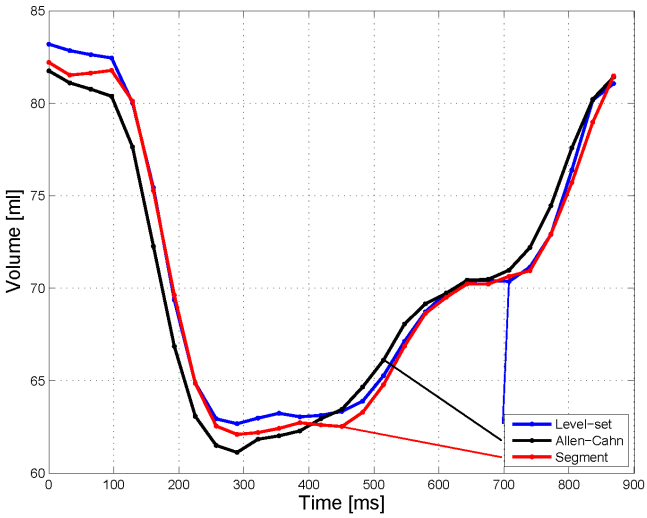

Fig. 9. Subject 5: Estimate of the LV volume during the heart cycle.

heart cycle. We present the results of fully automated segmentation, i. e. no manual corrections are needed. Nevertheless, the first initial condition p_{ini} must be placed by its level set $p = \frac{1}{2}$ inside the LV cavity manually and p_{ini} of next slices and time frames are given by the segmentation result of the neighboring slice or time frame. The algorithm is not sensitive to the shape of the p_{ini}. Usually, we start the segmentation with the end-systolic time frame in an apical slice. Then, each slice in time and space is segmented by algorithm (3). The segmentation parameters are adjusted according to Section 4.

In Figures 2 – 4, the selected heart images of the examined subjects are presented. The images were obtained using the bSSFP sequence. The algorithm is robust in processing of the bSSFP data and does not need any corrections in the segmentation.

In Figure 2, the evolution of the segmentation curve of the examined Subject 1 is shown. The initial guess p_{ini} is placed manually inside the LV cavity (Figure 2a). Figures 2b – 2d present the shape of segmentation curve after 100, 400 and 970 iterations steps.

In Figure 3, the selected time frames from the given spatial slice of the examined Subject 3 are shown. Figures 3a – 3d present the frames 03, 09, 11 and 22. The time frame 09 corresponds to the end-systolic phase whereas the time frame 22 corresponds to the end diastolic phase. As it can be seen in Figure 3d, the papillary muscle is detected by the algorithm and is not included in the LV volume. This result is achieved due to the sensitive choice of the external force (5).

In Figure 4, the selected spatial slices with the same time frame number of the examined Subject 5 are shown. Figures 4a – 4d present the slices 04, 06, 07, 10. The slice 04 is located near the heart base, whereas the slice 10 belongs to the heart apex. As in Figure 3d we can see that in Figure 4a the papillary muscle is detected as well.

Knowing the distance between the neighboring slices along the long axis and having segmented all of them, we can provide an estimate of the LV volume for each time

frame. In Figures 5 – 9, the graphs of the LV volume versus time are shown for Subjects 1 – 5. The results of the LV cavity segmentation using the algorithm based on the Allen–Cahn equation (black solid line) are compared to both the algorithm using the level-set approach (blue solid line) and the software package SEGMENT with manual corrections (red solid line).

Using the estimated values of the LV volume, the LV ejection fraction EF is calculated as follows

$$EF = \frac{EDV - ESV}{EDV},$$

where EDV stands for the end-diastolic LV volume (the volume of fully filled ventricle) and ESV stands for the end-systolic LV volume (the volume of the blood that remains in the ventricle after the ejection phase). Tables 4 – 5 show the ejection fraction, end-systolic LV volume and end-diastolic LV volume obtained by each of the compared algorithms.

7. DISCUSSION

The cardiac MRI data segmentation is an important part of the MR data post-processing. In the discussed application, the number of acquired images in a single examination exceeds 200. This number is very large for a manual segmentation. Therefore, the automated segmentation becomes useful despite of the character of cardiac MR images (limited signal-to-noise and contrast-to-noise ratio, motion and pulsation artifacts).

The presented algorithm is applied to 2D data in the form of particular slices of the cardiac MRI structured vertically. This data is dynamically recorded within the cardiac cycle. Sofar, the MRI technology allows to work with kinetic cardiac data within these limits in clinical applications. The fully 3D MRI data acquisition is nowadays possible using a breath-navigator technique. However, it does not yield functional images of the whole cardiac cycle, but only one – typically diastolic – image. Clinically, its usage is also limited due to the long acquisition times.

As the quality of cine MRI obtained by the bSSFP sequence is high within the cardiac cycle, the segmentation of the *left ventricle* can start at the end-systolic images, and the result can be propagated backwards and forwards in time. The inter-slice propagation for the end-systolic images is efficient provided a non-constant force F is used according to Section 4.2. The automated segmentation of the whole heart yields an acceptable agreement with other methods as indicated in Section 6. Ideally, only one end-systolic time frame in the first slice has to be treated manually. This means one manual placement of p_{ini} per hundreds of images segmented automatically afterwards.

The detection of the inner contour in the mid-ventricle slices is difficult due to the presence of *papillary muscles*. Although they are easily distinguishable in the end-diastolic scans, it is sometimes impossible to distinguish them in the scans of the contracted heart since the muscles are in a close contact with the ventricle wall (see the position of papillary muscles during the systole and the diastole in Figure 1).

The *signal-to-noise ratio* of the image can be increased by pre-processing of the segmented image P_0 by the convolution with the Gaussian kernel, which can be viewed as the solution of the linear diffusion equation. Such a process causes smoothing in all

directions which is not optimal for the edge detection. Therefore, it is more convenient to apply some non-linear types of diffusion that preserve sharp edges, see [21].

The stopping criterion suggested in Section 4.3 is used instead of other known criteria (see [22]) since it was easy to implement, fast to perform and successful in results. The restricted temporal resolution of the MR device causes *image blurring* during the period of the fastest part of the ventricle contraction. The inner contour of the ventricle may become indistinguishable even for the naked eye. The stopping criterion with the limited maximum number of iterations can still provide satisfactory results.

8. CONCLUSION

The cardiac MRI data segmentation is an important part of the MR data post-processing. The data set of each examination is large, and requires a certain level of automated examination. However, data quality (a limited signal-to-noise and contrast-to-noise ratio, motion and pulsation artifacts) makes the fully automated segmentation difficult. For this purpose, a nonlinear diffusion segmentation algorithm is used, which is justified by the mathematical and physical origin. This allows to refine the selection of segmentation parameters for images with a variable quality. The article summarizes the results related to the estimation of the LV volume through the whole cardiac cycle and estimation of the LV ejection fraction.

The described method can successfully approximate the dynamics of the LV volume. It operates automatically, however it usually requires the manual placement of p_{ini} for one image in the examination data set in order to select the segmented domain, i. e. the LV cavity. The algorithm is robust with respect to the used parameters.

The algorithm segments a single image in about 10 seconds[1] on Intel® Core™i5 CPU 2.67GHz. The processing of images for one examined subject requires the CPU time of tens of minutes, within the given implementation. The CPU efficiency still could be improved by means of parallelization or implementation on GPU.

In conclusion, reduction of manual operations with the MRI to a necessary minimum using a transparent, physically justified, robust and controllable method belong to the main advantages of the algorithm. Still longer processing times for one examined subject and the initial manual setup represent a challenge for further development of this approach.

ACKNOWLEDGMENT

This work was partially supported by the project MŠMT No. MSM6840770010 (Applied Mathematics in Technical and Physical Sciences), the project of the Czech Technical University in Prague No. SGS11/161/OHK4/3T/14 (Advanced Supercomputing Methods for Implementation of Mathematical Models) and by the projects MŠMT 1M6798582302, MZO 00023001, Czech Republic. The authors thank to the MR departments of the hospital IKEM Prague for providing MR image data.

(Received September 2, 2011)

[1]Using the numerical grid with 256×256 degrees of freedom, time step $\tau = 1.5 \times 10^{-}5$, 1000 time iterations. With the a priori knowledge of the segmented neighboring image, usually not more than 200–300 iterations are needed.

REFERENCES

[1] S. Allen and J. W. Cahn: A microscopic theory for antiphase boundary motion and its application to antiphase domain coarsening. Acta Metall *27* (1979), 1084–1095.

[2] M. Beneš: Mathematical analysis of phase-field equations with numerically efficient coupling terms. Interfaces and Free Boundaries *3* (2001), 201–221.

[3] M. Beneš, V. Chalupecký, and K. Mikula: Geometrical image segmentation by the Allen–Cahn equation. Appl. Numer. Math. *51* (2004), 2, 187–205.

[4] M. Beneš, R. Chabiniok, M. Kimura, and K. Mikula: Nonlinear Gauss–Seidel scheme for Allen–Cahn type systems. In: MAGIA 2007 (Mathematics, Geometry and Their Applications)(M. Vajsáblová and P. Struk, eds.), Publishing House of Slovak Technical University, Bratislava 2008, pp. 29–35.

[5] J. Bogaert, S. Dymarkowski, and A. M. Taylor: Clinical Cardiac MRI. Springer, Berlin – Heidelberg 2005.

[6] A. Bovik (ed): Handbook of Image and Video Processing. Academic Press, San Diego 1990.

[7] Y. Boykov, O. Veksler, and R. Zabih: Fast approximate energy minimization via graph cuts. IEEE Trans. Pattern Analysis and Machine Intelligence *23* (2001), 1222–1239.

[8] M. D. Cerqueira, N. J. Weissman, V. Dilsizian et al.: Standardized myocardial segmentation and nomenclature for tomographic imaging of the heart: A statement of healthcare professionals from the Cardiac Imaging Comittee of the Council on Clinical Cardiology of the American Heart Association. Circulation *105* (2002), 539–542.

[9] Y. Cheng: Mean shift, mode deeking, and clustering. IEEE Trans. on Pattern Analysis and Machine Intelligence *17* (1995), 790–799.

[10] M. G. Crandall, H. Ishii, and P. L. Lions: User's guide to viscosity solutions of second order partial differential equations. Bull. Amer. Math. Soc. *27* (1992), 1–67.

[11] S. Geman and D. Geman: Stochastic relaxation, Gibbs distribution, and the Bayesian restoration of images. IEEE Trans. on Pattern Analysis and Machine Intelligence *6* (1984), 721–741.

[12] E. Heiberg, L. Wigstrom, M. Carlsson, A. F. Bolger, and M. Karlsson: Time resolved three-dimensional automated segmentation of the left ventricle. In: Proc. IEEE Computers in Cardiology 2005 (32), Lyon 2005, pp. 599–602.

[13] E. Heiberg, J. Sjögren, M. Ugander, M. Carlsson, H. Engblom, and H. Arheden: Design and validation of SEGMENT – a freely available software for cardiovascular image analysis. BMC Medical Imaging *10* (2010), 1.

[14] M. Kass, A. Witkin, and D. Terzopoulos: Snakes: Active contour models. Internat. J. Computer Vision *1* (1988), 321–331.

[15] R. Máca, M. Beneš, and J. Tintěra: Degenerate diffusion methods in computer image processing and application. J. Math-for-Industry *3* (2011), 33–40.

[16] R. Malladi, J. A. Sethian, and B. Vemuri: Shape modeling with front propagation: A level set approach. IEEE Trans. on Pattern Analysis and Machine Intelligence *17* (1995), 2, 158–175.

[17] K. Mikula, A. Sarti. and F. Sgallari: Co-volume level set method in subjective surface based medical image segmentation. In: Handbook of Medical Image Analysis: Segmentation and Registration Models (J. Suri et al., eds.), Springer, New York 2005, pp. 583–626.

[18] D. Mumford and J. Shah: Boundary detection by minimizing functionals. In: Proc. IEEE Conference on Computer Vision and Pattern Recognition 1985, pp. 22–26.

[19] S. Osher and R. Fedkiw: Level Set Methods and Dynamic Implicit Surfaces. Springer Verlag, New York 2003.

[20] N. Paragios, Y. Chen, and O. Faugeras: Handbook of Mathematical Models of Computer Vision. Springer, New York 2005.

[21] P. Perona and J. Malik: Scale space and edge detection using anisotropic diffusion. IEEE Trans. on Pattern Analysis and Machine Intelligence *12* (1990), 629–639.

[22] H. K. Zhao, S. Osher, T. Chan, and B. Merriman: A variational level set approach to multiphase motion. J. Comput. Phys. *127* (1996), 179–195.

[23] S. Zhu and A. Yuille: Region competition: Unifying snakes, region growing, and Bayes/Mdl for multiband image segmentation. IEEE Trans. on Pattern Analysis and Machine Intelligence *18* (1996), 884–900.

Radomír Chabiniok, Imaging Sciences & Biomedical Engineering Division, Rayne Institute, St. Thomas Hospital, King's College, Strand, WC2R 2LS London. United Kingdom.
e-mail: radomir.chabiniok@kcl.ac.uk

Radek Máca, Department of Mathematics, Faculty of Nuclear Sciences and Physical Engineering, Czech Technical University Prague, Trojanova 13, 120 00 Praha 2. Czech Republic.
e-mail: radek.maca@fjfi.cvut.cz

Michal Beneš, Department of Mathematics, Faculty of Nuclear Sciences and Physical Engineering, Czech Technical University Prague, Trojanova 13, 12 00 Praha 2. Czech Republic.
e-mail: michal.benes@fjfi.cvut.cz

Jaroslav Tintěra, Institute of Clinical and Experimental Medicine, Vídeňská 1958/9, 140 21 Praha 4. Czech Republic.
e-mail: Jaroslav.Tintera@medicon.cz